Cobalt chloride has beneficial effects across species through a hormetic mechanism

Alfonso Schiavi[1,2†], Alessandra Runci[1,2†], Teresa Maiorino[3‡], Francesco Davide Naso[3], Marta Barenys[1‡], Ellen Fritsche[1], Flavie Strappazzon[3,4] and Natascia Ventura[1,2]*

[1]Institute of Clinical Chemistry and Laboratory Diagnostic, Medical Faculty, Heinrich Heine University, Düsseldorf, Germany, [2]Leibniz Research Institute for Environmental Medicine (IUF), Düsseldorf, Germany, [3]IRCCS Santa Lucia Foundation, Rome, Italy, [4]Institut NeuroMyogène, CNRS UMR5261—INSERM U1315, Université Claude Bernard Lyon1, Lyon, France

Severe oxygen and iron deficiencies have evolutionarily conserved detrimental effects, leading to pathologies in mammals and developmental arrest as well as neuromuscular degeneration in the nematode *Caenorhabditis elegans*. Yet, similar to the beneficial effects of mild hypoxia, non-toxic levels of iron depletion, achieved with the iron chelator bipyridine or through frataxin silencing, extend *C. elegans* lifespan through hypoxia-like induction of mitophagy. While the positive health outcomes of hypoxia preconditioning are evident, its practical application is rather challenging. Here, we thus test the potential beneficial effects of non-toxic, preconditioning interventions acting on iron instead of oxygen availability. We find that limiting iron availability through the iron competing agent cobalt chloride has evolutionarily conserved dose-dependent beneficial effects: while high doses of cobalt chloride have toxic effects in mammalian cells, iPS-derived neurospheres, and in *C. elegans*, sub-lethal doses protect against hypoxia- or cobalt chloride-induced death in mammalian cells and extend lifespan and delay age-associated neuromuscular alterations in *C. elegans*. The beneficial effects of cobalt chloride are accompanied by the activation of protective mitochondrial stress response pathways.

KEYWORDS

aging, *C. elegans*, cobalt chloride, iron, healthspan, hormesis, neurodegeneration

Introduction

Severe hypoxia has evolutionarily conserved and widely described deleterious consequences, ranging from ischemic stroke and myocardial infarction in mammals to developmental arrest and neuromuscular degeneration in the nematode *Caenorhabditis elegans* (*C. elegans*) (Rodriguez et al., 2013; Lee et al., 2019). In normoxic conditions, HIF1α (hypoxia-inducible-factor) is hydroxylated by enzymes that require O_2, Fe^{++}, and 2-oxoglutarate: at proline by PHD1-3 (prolyl-4-hydroxylase

domain-containing enzymes) or at asparagine by FIH (factor inhibiting HIF). This leads to the subsequent ubiquitination and degradation of HIF1α via the proteasome. Low oxygen and iron concentrations diminish PHD and FIH hydroxylase activities and prevent HIF1α degradation. This favors HIF1α translocation into the nucleus and binding to co-activators, which ultimately induces its transcriptional activity resulting in the modulation of a variety of downstream genes containing hypoxia response elements (HRE) (Wenger, 2002; Powell-Coffman, 2010). Accordingly, iron chelators such as deferoxamine (DFO) or bipyridine (BP), and iron-competing metals such as cobalt chloride (CoCl$_2$) or nickel chloride (NiCl$_2$) have been shown to work as hypoxia mimetics by deactivating the hydroxylases (Goldberg et al., 1988). Furthermore, similar to severe hypoxia, severe iron depletion is also involved in the pathogenesis of different human disorders and it leads to developmental arrest in *C. elegans* (Schiavi et al., 2015; Schiavi et al., 2020). Iron is an essential factor for several enzymes and cellular reactions, and therefore, its homeostasis must be finely tuned. Not only iron deprivation but also its excessive accumulation has evolutionarily conserved detrimental effects. Iron overload concurs to the pathogenesis of age-associated neuronal pathologies such as Parkinson's or Alzheimer's diseases, and it is a typical hallmark of the aging process, thereby shortening lifespan in *C. elegans* (Lee et al., 2006; Schiavi et al., 2015).

Friedreich's ataxia (FRDA) is the most frequently inherited recessive ataxia, and it is ascribed to severe deficiency of frataxin, a nuclear-encoded mitochondrial protein involved in iron–sulfur cluster (ISC) protein biogenesis and iron homeostasis. Accumulation of iron within mitochondria, with consequent alteration of ISC formation and induction of a cytosolic iron-starvation response, has been recognized as a consequence of frataxin deficiency involved in disease pathogenesis (Anzovino et al., 2014). In line with the disease state, and similar to severe oxygen and iron deprivation, severe or complete frataxin deficiency also displays evolutionarily conserved detrimental effects, leading to lethality in mice and to developmental arrest in *C. elegans* (Puccio et al., 2001; Ventura et al., 2005). Nonetheless, non-toxic levels of iron depletion, achieved with the iron chelator BP or through frataxin (*frh-1*) silencing, extend *C. elegans* lifespan through hypoxia-like induction of mitophagy (Schiavi et al., 2015). Moreover, exposure to non-lethal levels of hypoxia (or hypoxia preconditioning, HP) has been shown to prevent the detrimental effects of severe hypoxia-induced neuronal degeneration in an evolutionarily conserved manner (Dasgupta et al., 2007; Liu et al., 2021). While the potential beneficial health effects of HP are evident, its actual exploitation is hampered by the low feasibility of its practical application. In this study, we thus asked whether

FIGURE 1
(A–H) Representative pictures and quantification of neuronal differentiation **(A–D)** and necrotic cell death **(E–H)** of mouse embryo iPS-derived neurospheres left untreated or treated with cobalt chloride 600 µM (CoCl—600 µM) **(A–F)** for 48 h, deferoxamine 500 µM (DFO 500 µM) **(C,G)** for 72 h, or 2,2′-dipyridyl 500 µM (BP 500 µM) **(D,F)** for 72 h during neuronal precursor cells (NPC) differentiation. Bar graph represents means ± SEM from n = 3 independent replicas where N = 5 randomly chosen fields were scored. Unpaired t-test, *p value < 0.05 and **p value < 0.01 versus untreated. Above the bar graphs are shown the representative fluorescence pictures of the corresponding conditions. Scale bar are 100 µm. Green fluorescence pictures show neurons stained with beta-III-tubulin **(A)**, and blue fluorescence pictures show nuclei stained with Hoechst 33342 **(E)**.

non-toxic, preconditioning interventions acting on iron instead of oxygen availability may provide beneficial effects too. We found that similar to HP, limiting iron availability through CoCl$_2$ treatment has evolutionarily conserved beneficial effects, protecting against severe hypoxia- and age-induced neuromuscular alterations. We thus provide evidence that limiting iron availability represents a potential feasible strategy to delay aging and associated neuromuscular pathologies possibly *via* autophagy/mitophagy induction.
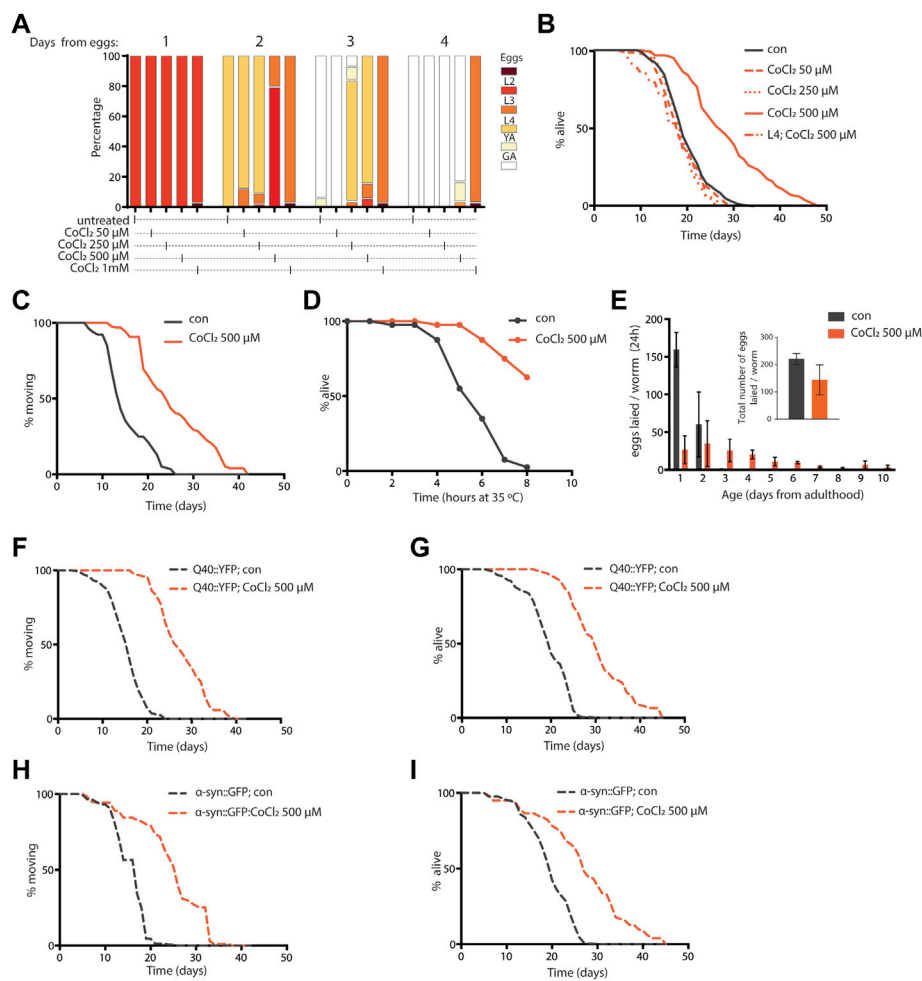
FIGURE 2
(A) Developmental rate of wild-type animals—from eggs through four different larval stages, until young (YA), and finally gravid (GA) adults—either left untreated or treated from eggs with 50 µM, 250 µM, 500 µM, and 1 mM cobalt chloride (CoCl$_2$ 50 µM, CoCl$_2$ 250 µM, CoCl$_2$ 500 µM, and CoCl$_2$ 1 mM), and followed for 4 days after hatching at 20°C. **(B)** Kaplan−Meier survival curves at 20°C of wild-type worms, left untreated (con) or treated from eggs with 50 µM, 250 µM, and 500 µM CoCl$_2$ and starting from L4 larval stage with 500 µM CoCl$_2$. Comparison between curves was performed using the log-rank test (Table 1). **(C,D)** Animals' locomotion activity **(C)** and survival against heat shock **(D)** of wild-type strain left untreated (con) or treated with 500 µM cobalt chloride (CoCl$_2$ 500 µM). Comparison between curves was performed using the log-rank test. **(E)** Fertility and brood size over time of wild-type worms treated as in (C). **(F−I)** Animal locomotion activity **(F,H)** and survival against heat shock **(G,I)** of *unc-54p*::Q40::YFP **(F,G)** or *unc-54p*::a-syn::YFP **(H,I)** strain left untreated (con) or treated with 500 µM cobalt chloride (CoCl$_2$ 500 µM). Comparison between curves was performed using the log-rank test.

Results

Cobalt chloride promotes healthspan in *C. elegans*

Iron is a vital cofactor for numerous proteins and enzymatic reactions and its intracellular concentration has to be finely tuned for appropriate organism homeostasis (Schiavi et al., 2020). Accordingly, both excess iron accumulation and depletion have toxic effects across species. Interestingly, we have previously shown that contrary to its severe deficiency, sub-

lethal iron depletion through the iron chelator BP or through *frh-1* silencing extends *C. elegans* lifespan (Schiavi et al., 2015). Limiting iron availability acts as a hypoxia mimetic, and exploiting hypoxia mimetics to prevent or protect against hypoxia- or age-induced neuromuscular pathologies may provide different advantages over hypoxia preconditioning. We thus sought to investigate the beneficial effects of additional modulators of iron availability. Consistent with the detrimental role of severe iron depletion especially during development, we found that the iron chelators DFO and BP as well as the iron-competing metal CoCl$_2$ significantly reduce

TABLE 1 Summary of lifespan analysis.

Genotype	Treatment	Mean lifespan (days)	Standard error	p vs. con	Age at 100% mortality (days)	Total/ censor	N
Wild-type (N2)	Con	19.8	0.4		34	275/22	4
	CoCl$_2$ 500 µM	28.6	0.7	<0.0001	48	195/41	3
	CoCl$_2$ 250 µM	19.6	0.4	0.9	28	145/19	2
	CoCl$_2$ 50 µM	20.3	0.7	1	30	145/47	2
	CoCl$_2$ 500 µM/L4	17.6	0.9	0.9	26	130/97	2
AM141 (unc-54p:: Q40::YFP)	Con	19.5	0.4		30	195/24	3
	CoCl$_2$ 500 µM	30.6	0.6	<0.0001	45	195/76	3
NL5901 (unc-54p:: αsyn::YFP)	Con	19.7	0.4		30	195/22	3
	CoCl$_2$ 500 µM	27.4	0.8	<0.0001	45	195/86	3

neuronal differentiation (Figures 1A–D) and viability (Figures 1E–H) in mouse neural progenitor cell (NPC)-derived neurospheres, a very sensitive and powerful system for developmental neurotoxicity studies (Fritsche et al., 2018).

Similar to complete *frh-1* deficiency (Ventura et al., 2005) or high doses of BP (Schiavi et al., 2015), a high concentration of CoCl$_2$ also arrested development in *C. elegans* (Figure 2A). Most notably, we found that non-toxic doses of CoCl$_2$ extend lifespan and healthspan (motility period) in a stage- and dose-dependent manner (Figures 2B,C; Table 1). This is in line with what has been previously observed with BP treatment or depletion of different mitochondrial electron transport chain (ETC) regulatory proteins including *frh-1* (Dillin et al., 2002; Rea et al., 2007; Schiavi et al., 2015). Pro-longevity doses of CoCl$_2$ also significantly reduced the animals' size (Supplementary Figure S1), increased their resistance to heat shock (Figure 2D), and extended their fertility period without modifying the overall brood size (Figure 2E). These are all parameters also associated with mitochondrial-stress extension of lifespan.

Excess iron is a typical hallmark of the aging process which concurs to the pathogenesis of age-associated neurodegenerative diseases, and progressive accumulation and toxicity of aggregation-prone proteins in these diseases are worsened by excess iron levels (Lee and Andersen, 2006; Schiavi et al., 2020). We thus wondered whether CoCl$_2$ could promote beneficial effects in *C. elegans* strains expressing human aggregation-prone proteins, poly-Q40 and α-synuclein (under muscle-specific promote, *unc-54*), and widely exploited as model systems to respectively study Huntington's and Parkinson's diseases (Alexander et al., 2014; Caldwell et al., 2020; Liang et al., 2020). Notably, CoCl$_2$ also significantly extended lifespan and locomotion ability in the Huntington's and Parkinson's disease models (Figures 2F–I). Moreover, we observed an age-dependent accumulation of poly-Q40 and α-synuclein aggregates, which was significantly reduced by pro-longevity CoCl$_2$ treatment (Supplementary Figure S1). Thus, in

C. elegans, CoCl$_2$ extends health- and lifespan in a wild-type background as well as in age-associated disease models.

Cobalt chloride activates mitochondrial stress response pathways in *C. elegans*

Given the striking similarity between animals' phenotypes upon CoCl$_2$ treatment and pro-longevity mitochondrial stress (Rea et al., 2007; Ventura et al., 2009), we then wondered whether the beneficial effects of CoCl$_2$ preconditioning in *C. elegans* could be ascribed to the induction of mitochondrial stress response signaling. Interestingly, like *frh-1* silencing (Ventura et al., 2009; Schiavi et al., 2015), pro-longevity doses of CoCl$_2$ in *C. elegans* significantly increased the expression of genes normally induced by mitochondrial stress such as *gst-4* (glutathione-S-transferase), *hsp-6* (mitochondrial unfolded protein response), and *nhr-57* (hypoxia–inducible gene) and reduced the expression of the mitophagy marker *dct-1*/BNIP3 (Figures 3A–D). CoCl$_2$ also strongly induced the nuclear translocation of the autophagy regulator transcription factor *hlh-30*/TFEB, but only marginally affected the number of *lgg-1*/LC3 and of *sqst-1*/p62 foci, the other two central autophagy regulatory genes (Figures 3E–G). These changes suggest CoCl$_2$ treatment induces mitochondrial stress that activates the autophagic machinery.

In mammals, Bnip3/*dct-1*-regulated mitochondrial autophagy is induced in response to hypoxia in a HIF-1-dependent manner (Zhang et al., 2008; Bellot et al., 2009), and in *C. elegans*, *frh-1* silencing extends lifespan *via* mitophagy activation and in a *hif-1*-dependent manner (Schiavi et al., 2015). Here, we find that the *C. elegans* HIF-1 homolog, *hif-1*, is required for the survival of CoCl$_2$-treated animals. Indeed, while *C. elegans* wild-type animals treated with pro-longevity doses of CoCl$_2$ reached the fertile stage slower than untreated animals (Figure 2A), *hif-1* mutants
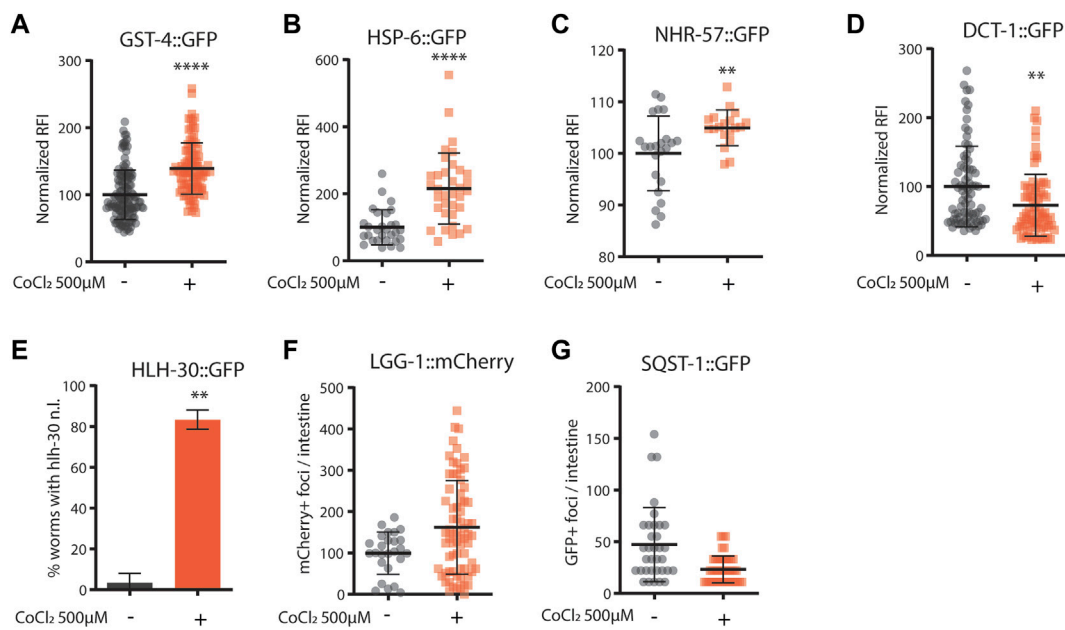
FIGURE 3
(A–G) Quantification of fluorescence reported strains in adult worms (4 days old) left untreated (−) or treated from eggs with CoCl₂ 500 μM (+).
Relative fluorescence intensity normalized to animals' size was quantified in GST-4::GFP **(A)**, HSP-6::GFP **(B)**, NHR-57::GFP **(C)**, and DCT-1::GFP **(D)**.
Percentage of worms with HLH-30::GFP nuclear localization **(E)**. Fluorescence foci number was quantified in LGG-1: mCherry **(F)** and SQST-1::GFP
(G). Bar graph represents means ± SD (n = 3, N = 10−15); lines in the scatter plots represent means ± SD (n = 3, N = 10−15). Comparison between
con and CoCl₂ was performed using the unpaired t-test. **p value < 0.01 and **** p value < 0.0001, versus con.
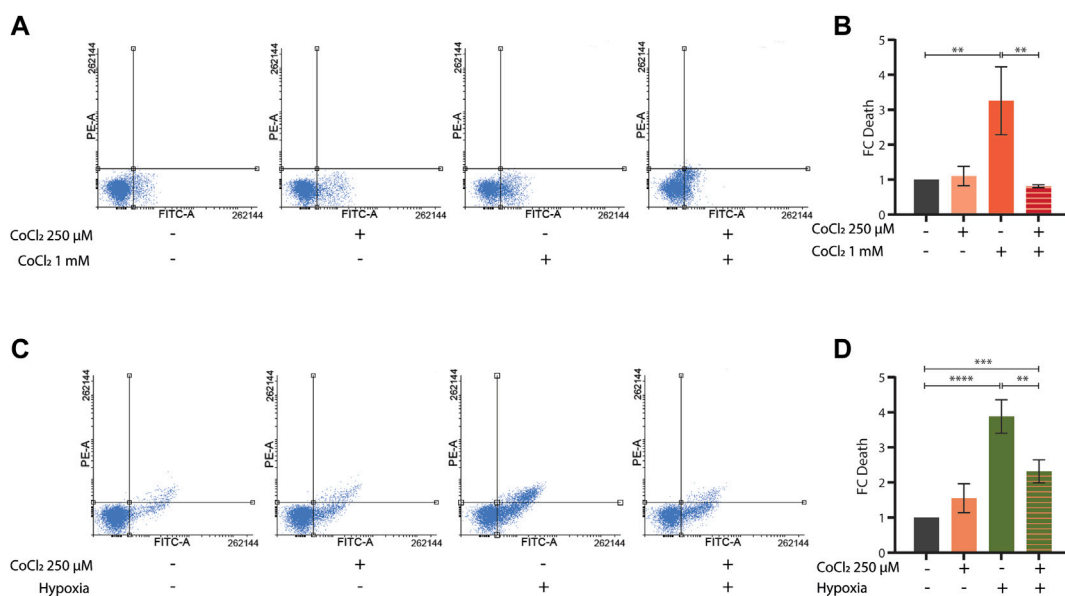
FIGURE 4
(A–D) Representative FACS plot **(A,C)** and quantification **(B,D)** of cell death assays performed in HeLa cells left untreated or treated with CoCl₂
1 mM for 48 h **(A,B)** or severe hypoxia (<1% O₂ for 48 h) **(C,D)** alone or in combination with either a CoCl₂ 250 μM pre-treatment for 24 h followed by
4 h recovery **(A,B)** or a CoCl₂ 250 μM co-treatment for 48 h, respectively. Bar graph represents means ± SD (n = 3); two-way ANOVA (Tukey's
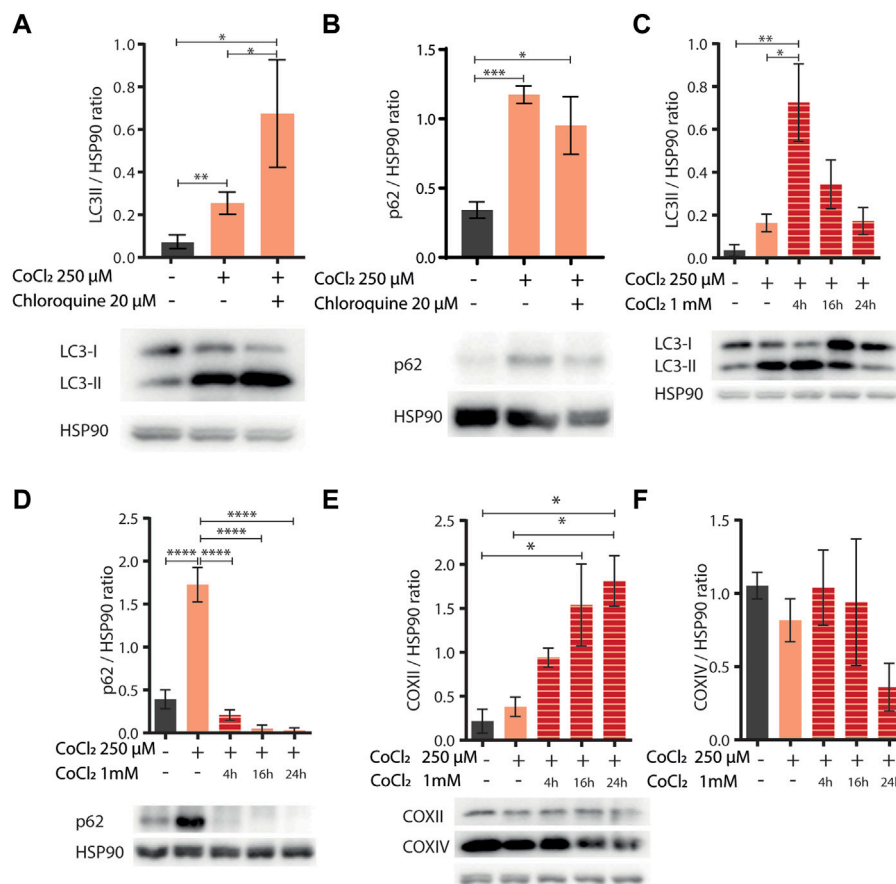multiple comparison test). **p value < 0.01 and **** p value < 0.0001.

FIGURE 5
(A,B) Western blot analysis of LC3II **(A)** and p62 **(B)** proteins extracted from HeLa cells left untreated (−) or treated (+) with 250 μM of CoCl$_2$ alone or in combination with 20 μM of chloroquine. Proteins were normalized using HSP90; below the bar graph are shown the representatives Western blot scan. Bar graphs represent means ± SD (N = 3), two-way ANOVA (Tukey's multiple comparison test). *p value < 0.05 and **p value < 0.01. **(C−F)** Western blot analysis of LC3II **(C)**, p62 **(D)**, and COXII **(E)** and COXIV **(F)** proteins extracted from HeLa cells left untreated (−) or treated (+) with 250 μM of CoCl$_2$ alone or in combination with 1 mM of CoCl$_2$ at different exposure time 4, 16, and 24 h. Proteins were normalized using HSP90, and below the bar graph **(C−E)** are shown the representatives Western blot scan. Bar graph represents means ± SD (N = 3), two-way ANOVA (Tukey's multiple comparison test). *p value < 0.05, **p value < 0.01, ***p value < 0.001, and ****p value < 0.0001.

completely arrested their development upon CoCl$_2$ treatment (Supplementary Figure S2). Thus, CoCl$_2$ activates a mitochondrial stress response likely in a *hif-1*-dependent manner.

Cobalt chloride preconditioning has beneficial effects across species

To further investigate the potential protective effects of CoCl$_2$ preconditioning, we then turned to mammalian cells. As expected, treatments with either high doses of CoCl$_2$ (1 mM for 48 h) or severe hypoxia (<0, 1% O$_2$ for 48 h) induced apoptosis in HeLa cells (Figures 4A,C). Notably, milder doses of CoCl$_2$ provided protection against apoptosis either when applied as a pretreatment (250 uM for 24 h, followed by a

recovery period of 4 h) before exposure to higher doses of CoCl$_2$ (Figures 4A,B) or when co-applied (250 uM for 48 h) during severe hypoxia treatment (Figures 4C,D).

Induction of autophagy and/or mitophagy is an attractive common determinant underlying the protection against aging and hypoxia induced by CoCl$_2$ preconditioning across species. Indeed, these fundamental cellular turnover processes are required to protect cells against hypoxia-induced cell death (Zhang et al., 2008) or against proteotoxicity (Florez-McClure et al., 2007; Guerrero-Gomez et al., 2019) and to extend *C. elegans* lifespan upon other iron depleting interventions such as *frh-1* RNAi or the iron chelator BP (Schiavi et al., 2013; Schiavi et al., 2015). Thus, to assess the effect of CoCl$_2$ preconditioning on autophagy activity, we analyzed the LC3II status [a well-known autophagosome marker (Klionsky et al., 2016)] by Western blot in mammalian cells, at early time points (before apoptotic cell

death was observed), upon mild doses of $CoCl_2$ either alone or in combination with chloroquine [CQ, an inhibitor of the fusion between autophagosomes and lysosomes used to ascertain the integrity of the autophagic flux (Klionsky et al., 2016)]. Mild doses of $CoCl_2$ significantly increased LC3II protein levels, which was further increased in the presence of CQ, thus clearly supporting the induction of intact autophagy flux by $CoCl_2$ preconditioning (Figure 5A). We then wondered whether mild doses of $CoCl_2$ also modulate the expression of p62/SQSTM1 protein, a targeted receptor for autophagic degradation of ubiquitinated substrates, which is often used as a reporter of autophagy activity (Klionsky et al., 2016). Surprisingly, LC3II accumulation upon $CoCl_2$ preconditioning was paralleled by a chloroquine-insensitive induction of p62 (Figure 5B). This indicates that the autophagic flux induced by $CoCl_2$ preconditioning is not sufficient to decrease the high levels of expression of p62 likely ascribed to a strong increase in its transcriptional expression and/or stability. Consistent with this possibility, exposure of preconditioned cells to higher doses of $CoCl_2$ (1 mM) significantly increased LC3 turnover at early time points and decreased p62 expression, indicating a strong induction of autophagy compared to $CoCl_2$ preconditioning alone (Figures 5C,D). The expressions of COXII and COXIV, two classical markers to reveal mitochondrial turnover (Klionsky et al., 2021), were instead inconsistently modulated (Figures 5E,F). To ascertain the effect of $CoCl_2$ preconditioning in prompting autophagy, we then compared the effect of 1mM $CoCl_2$ in HeLa cells pre-exposed or not to milder doses of $CoCl_2$. Our data confirmed that the preconditioning favors LC3II conversion compared to cells treated only with 1 mM CoCl2 as well as a stronger decrease of p62 (Supplementary Figures S3A,B). Moreover, we noticed that 1 mM CoCl2 alone stimulates the production of COXII and COXIV after 16 h of treatment (Supplementary Figures S3C,D). Notably, at this early time point used to analyze autophagy, we could already observe morphological changes hinting $CoCl_2$ preconditioning-induced protection in cells treated with 1 mM of $CoCl_2$ compared to cells undergoing only the severe treatment (Supplementary Figure S4). Thus, according to a hormetic paradigm, $CoCl_2$ preconditioning promotes healthspan likely *via* its hypoxia mimetic activity (compete with iron in HIF-1 activation), and autophagy induction may represent its underlying mechanism, which is in common with other treatments which limit iron availability (i.e., *frh-1* RNAi, BP).

Discussion

Overall, our work provides evidence that $CoCl_2$ preconditioning displayed evolutionarily conserved beneficial effects: it protects *C. elegans* against age- and proteotoxicity-induced neuromuscular damage and functional decline as well as mammalian cells against hypoxia-induced death. While we showed in the past that reducing the expression of the mitochondrial protein FRH-1 (*via frh-1* silencing) extends lifespan through an iron starvation response and in a *hif-1*-dependent manner, whether $CoCl_2$ promotes health span *via hif-1*-activation (through its iron competing effect) and/or also by inducing mitochondrial stress remains to be evaluated. Nonetheless, the ultimate effect of reducing iron availability is an improvement in health span, and this has important repercussions in light of the emerging role of hypoxia preconditioning in preventing neuromuscular deficits. Indeed, while the potential therapeutic benefits of hypoxia preconditioning are evident and have been suggested (Li et al., 2017; Caricati-Neto et al., 2019), fine-tuning oxygen levels to trigger beneficial effects without surpassing the critical threshold is not trivial and has low practical applications. Thus, the identification of more finely tunable interventions mimicking hypoxia, such as iron chelators already used in the clinic or undergoing clinical trials (Wijesinghe et al., 2021; Yang et al., 2021; Reddy et al., 2022) or modulators of downstream molecular players mediating their beneficial effects, may suggest more practicable strategies to interfere with the detrimental features associated with aging and severe hypoxia. Different phenotypic features are concurrently associated with the pro-longevity effect induced by mild doses of $CoCl_2$ such as reduced animals' size and egg-lay rate, prolonged fertility period, and increased resistance to stress (Ventura et al., 2005; Rea et al., 2007) and delayed neuromuscular decline during aging (Maglioni et al., 2014), which strikingly resemble those induced by mild mitochondrial stress. Notably, we showed that limiting iron availability with $CoCl_2$ displays beneficial effects only when applied at non-toxic doses. This threshold effect has been previously demonstrated for HP, mitochondria hormesis (e.g., with *frh-1* silencing), and the iron chelator BP, which only display beneficial properties at mild doses (Rea et al., 2007; Schiavi et al., 2015; Merry and Ristow, 2016; Li et al., 2017; Caricati-Neto et al., 2019). While HP has known beneficial effects against severe hypoxia-induced neuromuscular damage across species (Dasgupta et al., 2007), we show here that mild treatment with $CoCl_2$ may also similarly provide protection against severe hypoxia, aging, or accumulation of proteotoxic proteins. It is worth noting that the beneficial effect of the different iron depleting agents is dose-dependent and similar to mitochondrial stress (Dillin et al., 2002; Rea et al., 2007), it is elicited only when the agents are applied at sub-lethal doses starting during animal development. This clearly indicates that mitochondria preconditioning-associated metabolic remodeling must occur early in life to promote protection against aging and age-associated features (Maglioni et al., 2019).

In search of a common molecular mechanism mediating the beneficial effects of the different iron modulating interventions, we

initially considered *hif-1*-regulated autophagy or mitophagy. Indeed, autophagy protects against apoptosis (Marino et al., 2014) and against the toxicity of aggregation-prone proteins during aging (Florez-McClure et al., 2007; Guerrero-Gomez et al., 2019). Autophagy is also induced by hypoxia and by frataxin silencing across species and it is required to mediate the pro-longevity effect of *frh-1*-depletion in *C. elegans* (Schiavi et al., 2013; Schiavi et al., 2015). Our results in *C. elegans* clearly suggest that CoCl₂ acts in a *hif-1*-dependent manner. Moreover, the combined data in worms and cells support the induction of bulk autophagy as a likely downstream mediator of the beneficial effect of CoCl₂ preconditioning, but whether this is activated in a *hif-1*-dependent manner, *via* mitochondrial stress responses or other mechanisms, remains to be systematically investigated. Very interestingly, our data suggest that low doses of CoCl₂ "prepare" the cells for better autophagy activation by subsequent higher doses of hypoxia-like stress [which would otherwise have deleterious effects on the cells (Pourpirali et al., 2015)]. This is a classical hormetic scenario (Cypser and Johnson, 2002; Gems and Partridge, 2008), and it will be important to establish whether and how CoCl₂ preconditioning is also protective in other pathological or stressful contexts.

Paradoxically, our data point to a strong accumulation of p62 as a potential underlying mechanism of the CoCl₂ preconditioning effect. While an increase p62 may indicate a block of autophagy flux, which in a more severe hypoxic scenario (higher doses of CoCl₂) was linked to induction of apoptosis (Pourpirali et al., 2015), in our preconditioning paradigm, it could instead favor autophagy activation by additional stress. The overexpression of p62 by CoCl₂ preconditioning could be ascribed on the one hand to its increased stability *via* different post-translational modifications, which might prevent its association with the E3 ligase Keap1 (Kelch-like ECH-associated protein 1) followed by poly-ubiquitination and degradation in the proteasome (Pan et al., 2016; Sun et al., 2016; Xu et al., 2019; Feng et al., 2021). On the other hand, overexpression of p62 could be induced by transcriptional activation for instance by the redox transcription factor Nrf2 (nuclear factor erythroid 2-related factor 2). Since Nrf2 is also a substrate for Keap1, the binding of p62 to Keap1 results in a positive feedback loop leading to Nrf2 activation (Jain et al., 2010; Komatsu et al., 2010). Notably, we showed that CoCl₂ in *C. elegans* increases the expression of *gst-4* and of *dct-1*, two genes induced by mitochondrial stress in an Nrf2/*skn-1*-dependent manner (Ventura and Rea, 2007; Palikaras et al., 2015). While our combined findings in nematode and cells point to prompted activation of autophagy by CoCl₂ preconditioning followed by more severe treatment, they do not unambiguously support the induction of mitophagy. These results may be ascribed by the masking effects of cell-specific or cell-non-autonomous processes but also to context-specific roles of p62. Indeed, p62 is not always required to mediate mitophagy (Narendra et al., 2010) and it may also modulate other forms of cell death such as ferroptosis [e.g., *via* Nrf2 activation (Sun et al., 2020; Chen et al., 2022; Tang et al., 2022)].

Interestingly, while *frh-1* silencing induces both autophagy and mitophagy, the Nrf2/*skn-1* pathway and extends lifespan in a *hif-1*-dependent manner, the iron chelator BP only induces mitochondrial but not bulk autophagy, induces the Nrf2/*skn-1* pathway, and extends lifespan in a *hif-1*-independent manner (Schiavi et al., 2013; Schiavi et al., 2015). Moreover, while CoCl₂ modulates gene expression in a *hif-1*-dependent manner across species (Triantafyllou et al., 2006; Padmanabha et al., 2015), it can also induce hypoxia-regulated genes, such as *nhr-57*, in a *hif-1*-independent manner (Padmanabha et al., 2015). Thus, while reducing iron availability can mimic the beneficial effects of HP, the common underlying molecular mechanism of the different hypoxia-mimetics may in fact be through *hif-1*-independent but Nrf2-related pathways.

Further studies will be required to actually clarify whether autophagy, mitophagy, or other forms of iron-regulated processes such as ferritinophagy or ferroptosis are involved in the protective effects of CoCl₂ or other interventions reducing iron availability. In conclusion, we identified CoCl₂ as a new agent protecting against hypoxia- and age-induced neuromuscular degeneration, possibly *via hif-1*- and/or Nrf2-regulated pathways.

Materials and methods

Nematodes

C. elegans strains and culture conditions

The following strains were used in this study: N2 wild type, AM141: rmIs133 [*unc-54p*::Q40::YFP], NL5901: pkIs2386 [*unc-54p*::alpha-synuclein::YFP + *unc-119*(+)], CL2166: dvIs19 [pAF15(*gst-4p*::GFP::NLS)], SJ4100: zcIs13[*hsp-6p*::GFP], ZG120: ials07[*nhr-57p*::GFP, *unc-119*(+)], JIN1679: jinEx10 [*hlh-30p*::*hlh-30*::GFP + *rol-6*(*su1006*)], vkEx1093: [*nhx-2p*::mCherry::lgg-1], HZ589: bpIs151[*sqst-1p*::SQST-1::GFP; unc-76(+)]IV; him-5(e1490)V, IR1431: N2;Ex001[*dct-1p*::DCT-1::GFP], ZG31: *hif-1*(*ia4*).

All strains were maintained and kept synchronized by egg lay at 20°C on nematode growth media (NGM) agar supplemented with *Escherichia coli* OP50 unless otherwise described.

Chemical treatments

Cobalt chloride (CoCl2 C8661, Sigma-Aldrich) was dissolved at 0.1 M stock solution in ddH₂O, sterilized using a 0.22-μM filter, and supplemented to the NGM after autoclaving at the concentration of interest.

2,2′ dipyridyl (BP, 4153 Carl Roth) was dissolved in ddH₂O and added to NGM to the indicated concentrations.

Lifespan

Survival analyses were carried out with the standard procedure in the field as routinely carried out in our

laboratory (Torgovnick et al., 2018). Briefly, a synchronized population of 60–80 worms was used to start the lifespan analysis. Animals were transferred on fresh plates every day during the fertile phase and at the end of the fertile period, worms were transferred every other day. Animals not able to move upon prodding and with no pharyngeal pumping were scored as dead animals and were scored as not moving when no sinusoid locomotory activity was observed upon prodding. Survival analysis was performed in OASIS 2 using the Kaplan–Meier estimator. Statistical differences were evaluated using the log-rank test between the pooled population of worms, and p values were adjusted for multiple comparisons by the Bonferroni method.

Health span—movement

Movement was assessed in the same populations used for the lifespan assay. Worms able to crawl spontaneously or after manual stimulus were considered as moving, while dead worms or animals without crawling behavior were considered as not moving. Statistical analysis was performed as described for lifespan.

Fecundity

The fecundity of animals was estimated by counting the eggs laid in a period of 4 h; three worms on four different plates were used in each condition and repeated in three independent trials.

Heat shock resistance

Twenty wild-type animals for each condition were maintained from eggs at 20°C on plates with or without cobalt chloride 500 µM. On the first day of adulthood, they were moved to 35°C and the survival rate was counted every hour for 8 h.

Quantification of GFP-transgene expression by fluorescence microscopy

The nematodes were placed in a 15 µl S-Basal plus levamisole 10 mM drop on a microscope glass slide, covered with a cover slide, and immediately imaged. Pictures were acquired with an Imager 2 Zeiss fluorescence microscope, with magnification 25-fold. The images were analyzed with the software ImageJ (http://imagej.nih.gov/ij/). The bright field images were used to generate the mask to select each single worm pictured, and consequently to measure the fluorescence in the correspondent fluorescent filter.

Autophagy measurements

mCherry-positive foci from the Pnhx-2::mCherry::LGG-1 transgenic strain were counted in the intestine of young adult worms. To quantify p62::GFP puncta, the number of GFP foci was quantified in the anterior pharyngeal bulb of the Psqst-1:SQST-1::GFP transgenic strain. Worms were mounted on agarose pads, pictures were acquired using 100-fold magnification on a Zeiss Axio Imager

2 microscope, and the foci were analyzed with Fiji (Schindelin et al., 2012).

HLH-30 nuclear localization measurement

The number of worms showing HLH-30::GFP nuclear localization was visually counted using a Zeiss Axio Imager 2 (100-fold magnification). Worms were anesthetized using 10 mM levamisole in S-Basal and acquired within 5 min of mounting on glass slides. The percentage of worms with HLH-30 nuclear localization was calculated for each condition and plotted as mean ± SEM.

Poly-Q40 aggregation measurement

Poly-Q40 formations were acquired using a 25-fold magnification on a Zeiss Axio Imager 2 microscope. Worms were acquired at 4,7, and 10 days after hatching, and left untreated or treated from eggs with $CoCl_2$ 500 µM. The number of poly-Q40 aggregates was counted using the "analyze particles. . ." tools in ImageJ after thresholding and converting the acquired images in a binary form. The number of poly-Q40 was counted per worm by manually selecting the single worms. Worms were anesthetized using 10 mM levamisole in S-Basal and acquired within 5 min.

Mammalian systems

Cell line maintenance and treatment

The human cervix carcinoma (HeLa) cell line was used in this study. The cells were incubated at 37°C with 5% CO_2 and maintained in DMEM with 1.0 g/L glucose (PAN-Biotech GmbH, Germany) as a standard medium, supplemented with fetal bovine serum (FBS, Sigma-Aldrich), 10% and Penicillin/Streptomycin/Amphotericin B Mix (PAN-Biotech GmbH, Germany), 1%.

For cobalt chloride ($CoCl_2$ 15862, Sigma-Aldrich) treatment, it was directly added to the plates at the desired concentration. To generate the hypoxia status, the seeded cells were placed into a modular incubator chamber (Billups-Rothenberg). A gas mixture (95% N_2 and 5% CO_2) was flushed (15 l/min) into the chamber for 10 min and then incubated for the indicated time. After the different treatments, the cells were immediately collected for cell death detection.

Autophagosome–lysosome fusion was blocked with chloroquine (CQ) at 20 µM for 1 h (Sigma-Aldrich, United States). Images of HeLa cells after $CoCl_2$ treatments were acquired using the ZOE Fluorescent Cell Imager (Bio-Rad, United States).

Cell death detection by FACS analysis

HeLa cells, untreated or treated with cobalt chloride and/or hypoxia, were washed with PBS and collected by centrifugation after trypsinization. The cell pellet was suspended in binding buffer (Annexin V-FITC kit; BioVision, Milpitas, CA,

United States), followed by the addition of 5 µl Annexin V-labeling solution (BioVision) and 5 µl propidium iodide (BioVision). Cells were then incubated for 5 min at room temperature and analyzed *via* fluorescence-activated cell sorting (FACS; BD FACSCanto II).

Autophagy detection by Western blotting

HeLa cells were lysed in RIPA buffer (150 mM NaCl, 50 mM Tris with pH 7.4, 1% Triton, 0.5% Nonidet P40, 10% glycerol, and 2.5% sodium deoxycholate) plus protease and phosphatase inhibitors (Roche Diagnostic, Germany, 11836153001). Protein concentrations were determined with the Bio-Rad Protein Assay Dye kit (Bio-Rad, United States, 5000006). Cell extracts were resolved by SDS-PAGE and transferred onto PVDF membranes (Millipore, Germany, Immobilon-P IPVH00010). Blocking was performed at room temperature in TBS 1X 0.1% Tween 5% low-fat milk for 1 h. Membranes were incubated with primary antibodies overnight at +4°C, followed by incubation with horseradish peroxidase-conjugate secondary antibodies (Bio-Rad) and revealed with western chemoluminescent HRP substrate (Millipore, Immobilon WBKLS0500). Chemoluminescent signals were acquired with the iBright CL1000 Imaging System (Thermo Fisher, United States). Quantitative analysis was performed using ImageJ software. Primary antibodies used were rabbit anti-p62 (MBL International Corporation, United States, PM045), mouse anti-COXII (Abcam, United Kingdom, ab110258), mouse anti-COXIV (Abcam, United Kingdom, ab33985), rabbit anti-LC3 A/B (Cell Signaling, United States, D3U4C, 12741S), rabbit anti-HSP90 (Cell Signalling; United States, E289, 4875), and mouse anti-vinculin (Santa Cruz Biotechnology, United States, 7F9, sc-73614).

Mouse neural progenitor cell-derived neurosphere generation and treatment

Cryopreserved mouse neural progenitor cells were cultured at 37°C and 5% CO_2 as a suspension culture in a proliferation medium consisting of Dulbecco's modified Eagle medium (DMEM) supplemented with B27 (Invitrogen GmbH, Karlsruhe, Germany). When spheres reached 0.5 mm in diameter, they were chopped up to passage 3 with a McIlwain tissue chopper. Differentiation was initiated by growth factor withdrawal in a differentiation medium supplemented with N2 (insulin, transferrin, sodium selenite, putrescine, and progesterone; Invitrogen), plated onto poly-d-lysine/laminin–coated chamber slides (BD Bioscience, Erembodegem, Belgium). Cobalt chloride, deferoxamine, and 2,2′-dipyridyl were added at the desired concentration directly into the differentiation medium. The rate of neuronal differentiation and cell death were detected after 48 or 72 h of drug treatment.

Afterward, cells were fixed with 4% PFA (Sigma-Aldrich, Germany) for 30 min at 37°C and washed with PBS. Cells were stained with the primary antibody mouse-anti-βIII-tubulin for 1 h at 37°C. After washing with PBS, cells were incubated with the secondary antibody antimouse-Alexa-448 (Invitrogen,

United States) for 30 min at 37°C. Nuclei were stained with Hoechst 33258 (Sigma-Aldrich, Germany). Samples were analyzed using a fluorescent microscope (Carl Zeiss, Germany) and AxioVision Rel.4.8 software (Carl Zeiss, Germany).

For the quantification of neuronal differentiation, the number of βIII-tubulin + cells in a given area was manually counted and divided by the total number of nuclei of the same area, which were counted automatically with ImageJ, and the result was expressed in percentage. Afterward, the values obtained for all exposed groups were expressed in percentage of the value of the control of the corresponding experiment. Cell death (necrosis) quantification was performed by counting cells stained with propidium iodide normalized to the total number of cells stained with Hoechst.

Data availability statement

The raw data supporting the conclusions of this article will be made available by the authors, without undue reservation.

Author contributions

NV conceived and supervised the study. AS, AR, MB, FS, and NV designed the experiments. AS, AR, TM, FDN performed the experiments. AS, AR, FDN, TM, FS, and NV analyzed the data. AS and NV wrote the paper. FS and EF edited the manuscript.

Publisher's note

All claims expressed in this article are solely those of the authors and do not necessarily represent those of their affiliated organizations, or those of the publisher, the editors, and the reviewers. Any product that may be evaluated in this article, or claim that may be made by its manufacturer, is not guaranteed or endorsed by the publisher.

Conflict of interest

The authors declare that the research was conducted in the absence of any commercial or financial relationships that could be construed as a potential conflict of interest.

Acknowledgments

Supplementary material

The Supplementary Material for this article can be found online at: https://www.frontiersin.org/articles/10.3389/fcell.2022.986835/full#supplementary-material

SUPPLEMENTARY FIGURE S1
(A,B) Representative pictures **(A)** and quantification **(B)** of the poly-Q40 reporter strain AM141: rmIs133 [*unc-54p*::Q40::YFP] in 4-, 7-, and 10-days-old adult worms left untreated (−) or treated from eggs with CoCl$_2$ 500 μM (+). The number of poly-Q40 aggregates was counted using the "analyze particles. . ." tools in ImageJ after thresholding and converting the acquired images (right side of panel A) into a binary form (left side of

panel A). (B) Bar graph represents means $\pm$ SD (n = 3, N=10−15). Comparison between untreated and CoCl$_2$ at the same time point was performed using the unpaired t-test. *p value < 0.05 and **** p value < 0.0001. Scale bar = 100 μm.

SUPPLEMENTARY FIGURE S2
Developmental rate of wild-type (WT) and *hif-1* KO animals from eggs through four different larval stages, until young (YA) and gravid (GA) adults, either left untreated (−) or treated from eggs with 500 μM CoCl$_2$ (+) and followed for 5 days after hatching at 20°C.

SUPPLEMENTARY FIGURE S3
(A–D) Western blot analysis of LC3II **(A)**, p62 **(B)**, COXII **(C)**, and COXIV **(D)** proteins extracted from HeLa cells left untreated (−) or treated (+) with 250 μM alone or in combination with 1mM of CoCl$_2$ at different time points (4, 16, and 24 hours). Proteins were normalized using vinculin. Representative Western blots are shown. Bar graph represents means $\pm$ SD (N = 3). Comparison between groups was performed using the unpaired t-test. *p value < 0.05.

SUPPLEMENTARY FIGURE S4
Representative pictures of HeLa cells left untreated (−) or treated (+) with 250 μM alone or in combination with 1 mM of CoCl$_2$ (+) at different time points (4, 16, and 24 hours). White squares represent the magnified crop (2x) shown on the right. Scale bar = 100 μm.

References

Alexander, A. G., Marfil, V., and Li, C. (2014). Use of *Caenorhabditis elegans* as a model to study Alzheimer's disease and other neurodegenerative diseases. *Front. Genet.* 5, 279. doi:10.3389/fgene.2014.00279

Anzovino, A., Huang, M. L. H., and Richardson, D. R. (2014). Fixing frataxin: 'ironing out' the metabolic defect in friedreich's ataxia. *Br. J. Pharmacol.* 171 (8), 2174–2190. doi:10.1111/bph.12470

Bellot, G., Garcia-Medina, R., Gounon, P., Chiche, J., Roux, D., Pouyssegur, J., et al. (2009). Hypoxia-induced autophagy is mediated through hypoxia-inducible factor induction of BNIP3 and BNIP3L via their BH3 domains. *Mol. Cell. Biol.* 29 (10), 2570–2581. doi:10.1128/MCB.00166-09

Caldwell, K. A., Willicott, C. W., and Caldwell, G. A. (2020). Modeling neurodegeneration in *Caenorhabditis elegans*. *Dis. Model. Mech.* 13 (10), dmm046110. doi:10.1242/dmm.046110

Caricati-Neto, A., Errante, P. R., and Menezes-Rodrigues, F. S. (2019). Recent advances in pharmacological and non-pharmacological strategies of cardioprotection. *Int. J. Mol. Sci.* 20 (16), E4002. doi:10.3390/ijms20164002

Chen, J., Zhang, J., Chen, T., Bao, S., Li, J., Wei, H., et al. (2022). Xiaojianzhong decoction attenuates gastric mucosal injury by activating the p62/Keap1/Nrf2 signaling pathway to inhibit ferroptosis. *Biomed. Pharmacother.* 155, 113631. doi:10.1016/j.biopha.2022.113631

Cypser, J. R., and Johnson, T. E. (2002). Multiple stressors in *Caenorhabditis elegans* induce stress hormesis and extended longevity. *J. Gerontol. A Biol. Sci. Med. Sci.* 57 (3), B109–B114. doi:10.1093/gerona/57.3.b109

Dasgupta, N., Patel, A. M., Scott, B. A., and Crowder, C. M. (2007). Hypoxic preconditioning requires the apoptosis protein CED-4 in *C. elegans*. *Curr. Biol.* 17 (22), 1954–1959. doi:10.1016/j.cub.2007.10.017

Dillin, A., Hsu, A. L., Arantes-Oliveira, N., Lehrer-Graiwer, J., Hsin, H., Fraser, A. G., et al. (2002). Rates of behavior and aging specified by mitochondrial function during development. *Science* 298 (5602), 2398–2401. doi:10.1126/science.1077780

Feng, L., Chen, M., Li, Y., Li, M., Hu, S., Zhou, B., et al. (2021). Sirt1 deacetylates and stabilizes p62 to promote hepato-carcinogenesis. *Cell. Death Dis.* 12 (4), 405. doi:10.1038/s41419-021-03666-z

Florez-McClure, M. L., Hohsfield, L. A., Fonte, G., Bealor, M. T., and Link, C. D. (2007). Decreased insulin-receptor signaling promotes the autophagic degradation of beta-amyloid peptide in *C. elegans*. *Autophagy* 3 (6), 569–580. doi:10.4161/auto.4776

Fritsche, E., Barenys, M., Klose, J., Masjosthusmann, S., Nimtz, L., Schmuck, M., et al. (2018). Current availability of stem cell-based *in vitro* methods for

developmental neurotoxicity (DNT) testing. *Toxicol. Sci.* 165 (1), 21–30. doi:10.1093/toxsci/kfy178

Gems, D., and Partridge, L. (2008). Stress-response hormesis and aging: "that which does not kill us makes us stronger. *Cell. Metab.* 7 (3), 200–203. doi:10.1016/j.cmet.2008.01.001

Goldberg, M. A., Dunning, S. P., and Bunn, H. F. (1988). Regulation of the erythropoietin gene: Evidence that the oxygen sensor is a heme protein. *Science* 242 (4884), 1412–1415. doi:10.1126/science.2849206

Guerrero-Gomez, D., Mora-Lorca, J. A., Saenz-Narciso, B., Naranjo-Galindo, F. J., Munoz-Lobato, F., Parrado-Fernandez, C., et al. (2019). Loss of glutathione redox homeostasis impairs proteostasis by inhibiting autophagy-dependent protein degradation. *Cell. Death Differ.* 26 (9), 1545–1565. doi:10.1038/s41418-018-0270-9

Jain, A., Lamark, T., Sjottem, E., Larsen, K. B., Awuh, J. A., Overvatn, A., et al. (2010). p62/SQSTM1 is a target gene for transcription factor NRF2 and creates a positive feedback loop by inducing antioxidant response element-driven gene transcription. *J. Biol. Chem.* 285 (29), 22576–22591. doi:10.1074/jbc.M110.118976

Klionsky, D. J., Abdelmohsen, K., Abe, A., Abedin, M. J., Abeliovich, H., Acevedo Arozena, A., et al. (2016). Guidelines for the use and interpretation of assays for monitoring autophagy (3rd edition). *Autophagy* 12 (1), 1–222. doi:10.1080/15548627.2015.1100356

Klionsky, D. J., Abdel-Aziz, A K, Abdelfatah, S, Abdellatif, M, Abdoli, A, Abel, S, et al. (2021). Guidelines for the use and interpretation of assays for monitoring autophagy (4th edition)^1. *Autophagy* 17 (1), 1–382.doi:10.1080/15548627.2020.1797280

Komatsu, M., Kurokawa, H., Waguri, S., Taguchi, K., Kobayashi, A., Ichimura, Y., et al. (2010). The selective autophagy substrate p62 activates the stress responsive transcription factor Nrf2 through inactivation of Keap1. *Nat. Cell. Biol.* 12 (3), 213–223. doi:10.1038/ncb2021

Lee, D. W., Andersen, J. K., and Kaur, D. (2006). Iron dysregulation and neurodegeneration: The molecular connection. *Mol. Interv.* 6 (2), 89–97. doi:10.1124/mi.6.2.6

Lee, D. W., and Andersen, J. K. (2006). Role of HIF-1 in iron regulation: Potential therapeutic strategy for neurodegenerative disorders. *Curr. Mol. Med.* 6 (8), 883–893. doi:10.2174/156652406779010849

Lee, J. W., Ko, J., Ju, C., and Eltzschig, H. K. (2019). Hypoxia signaling in human diseases and therapeutic targets. *Exp. Mol. Med.* 51 (6), 1–13. doi:10.1038/s12276-019-0235-1

Li, S., Hafeez, A., Noorulla, F., Geng, X., Shao, G., Ren, C., et al. (2017). Preconditioning in neuroprotection: From hypoxia to ischemia. *Prog. Neurobiol.* 157, 79–91. doi:10.1016/j.pneurobio.2017.01.001

Liang, J. J. H., McKinnon, I. A., and Rankin, C. H. (2020). The contribution of *C. elegans* neurogenetics to understanding neurodegenerative diseases. *J. Neurogenet.* 34 (3-4), 527–548. doi:10.1080/01677063.2020.1803302

Liu, J., Gu, Y., Guo, M., and Ji, X. (2021). Neuroprotective effects and mechanisms of ischemic/hypoxic preconditioning on neurological diseases. *CNS Neurosci. Ther.* 27 (8), 869–882. doi:10.1111/cns.13642

Maglioni, S., Mello, D. F., Schiavi, A., Meyer, J. N., and Ventura, N. (2019). Mitochondrial bioenergetic changes during development as an indicator of *C. elegans* health-span. *Aging (Albany NY)* 11 (16), 6535–6554. doi:10.18632/aging.102208

Maglioni, S., Schiavi, A., Runci, A., Shaik, A., and Ventura, N. (2014). Mitochondrial stress extends lifespan in *C. elegans* through neuronal hormesis. *Exp. Gerontol.* 56, 89–98. doi:10.1016/j.exger.2014.03.026

Marino, G., Niso-Santano, M., Baehrecke, E. H., and Kroemer, G. (2014). Self-consumption: The interplay of autophagy and apoptosis. *Nat. Rev. Mol. Cell. Biol.* 15 (2), 81–94. doi:10.1038/nrm3735

Merry, T. L., and Ristow, M. (2016). Mitohormesis in exercise training. *Free Radic. Biol. Med.* 98, 123–130. doi:10.1016/j.freeradbiomed.2015.11.032

Narendra, D., Kane, L. A., Hauser, D. N., Fearnley, I. M., and Youle, R. J. (2010). p62/SQSTM1 is required for Parkin-induced mitochondrial clustering but not mitophagy; VDAC1 is dispensable for both. *Autophagy* 6 (8), 1090–1106. doi:10.4161/auto.6.8.13426

Padmanabha, D., Padilla, P. A., You, Y. J., and Baker, K. D. (2015). A HIF-independent mediator of transcriptional responses to oxygen deprivation in *Caenorhabditis elegans*. *Genetics* 199 (3), 739–748. doi:10.1534/genetics.114.173989

Palikaras, K., Lionaki, E., and Tavernarakis, N. (2015). Coordination of mitophagy and mitochondrial biogenesis during ageing in *C. elegans*. *Nature* 521, 525–528. doi:10.1038/nature14300

Pan, J. A., Sun, Y., Jiang, Y. P., Bott, A. J., Jaber, N., Dou, Z., et al. (2016). TRIM21 ubiquitylates SQSTM1/p62 and suppresses protein sequestration to regulate redox homeostasis. *Mol. Cell* 61 (5), 720–733. doi:10.1016/j.molcel.2016.02.007

Pourpirali, S., Valacca, C., Merlo, P., Rizza, S., D'Amico, S., and Cecconi, F. (2015). Prolonged pseudohypoxia targets Ambra1 mRNA to P-bodies for translational repression. *PLoS One* 10 (6), e0129750. doi:10.1371/journal.pone.0129750

Powell-Coffman, J. A. (2010). Hypoxia signaling and resistance in *C. elegans*. *Trends Endocrinol. Metab.* 21 (7), 435–440. doi:10.1016/j.tem.2010.02.006

Puccio, H., Simon, D., CosseeM.Criqui-FiliPe, P., TizianoF.Melki, J., et al. (2001). Mouse models for Friedreich ataxia exhibit cardiomyopathy, sensory nerve defect and Fe-S enzyme deficiency followed by intramitochondrial iron deposits. *Nat. Genet.* 27 (2), 181–186. doi:10.1038/84818

Rea, S. L., Ventura, N., and Johnson, T. E. (2007). Relationship between mitochondrial electron transport chain dysfunction, development, and life extension in *Caenorhabditis elegans*. *PLoS Biol.* 5 (10), e259. doi:10.1371/journal.pbio.0050259

Reddy, P. S., Locke, M., and Badawy, S. M. (2022). A systematic review of adherence to iron chelation therapy among children and adolescents with thalassemia. *Ann. Med.* 54 (1), 326–342. doi:10.1080/07853890.2022.2028894

Rodriguez, M., Snoek, L. B., De Bono, M., and Kammenga, J. E. (2013). Worms under stress: *C. elegans* stress response and its relevance to complex human disease and aging. *Trends Genet.* 29 (6), 367–374. doi:10.1016/j.tig.2013.01.010

Schiavi, A., Maglioni, S., Palikaras, K., Shaik, A., Strappazzon, F., Brinkmann, V., et al. (2015). Iron-starvation-induced mitophagy mediates lifespan extension upon mitochondrial stress in *C. elegans*. *Curr. Biol.* 25 (14), 1810–1822. doi:10.1016/j.cub.2015.05.059

Schiavi, A., Strappazzon, F., and Ventura, N. (2020). Mitophagy and iron: Two actors sharing the stage in age-associated neuronal pathologies. *Mech. Ageing Dev.* 188, 111252. doi:10.1016/j.mad.2020.111252

Schiavi, A., Torgovnick, A., Kell, A., Megalou, E., Castelein, N., Guccini, I., et al. (2013). Autophagy induction extends lifespan and reduces lipid content in response to frataxin silencing in *C. elegans*. *Exp. Gerontol.* 48 (2), 191–201. doi:10.1016/j.exger.2012.12.002

Schindelin, J., Arganda-Carreras, I., Frise, E., Kaynig, V., Longair, M., Pietzsch, T., et al. (2012). Fiji: An open-source platform for biological-image analysis. *Nat. Methods* 9 (7), 676–682. doi:10.1038/nmeth.2019

Sun, X., Ou, Z., Chen, R., Niu, X., Chen, D., Kang, R., et al. (2016). Activation of the p62-Keap1-NRF2 pathway protects against ferroptosis in hepatocellular carcinoma cells. *Hepatology* 63 (1), 173–184. doi:10.1002/hep.28251

Sun, Y., He, L., Wang, T., Hua, W., Qin, H., Wang, J., et al. (2020). Activation of p62-keap1-nrf2 pathway protects 6-hydroxydopamine-induced ferroptosis in dopaminergic cells. *Mol. Neurobiol.* 57 (11), 4628–4641. doi:10.1007/s12035-020-02049-3

Tang, K., Chen, Q., Liu, Y., Wang, L., and Lu, W. (2022). Combination of metformin and sorafenib induces ferroptosis of hepatocellular carcinoma through p62-keap1-nrf2 pathway. *J. Cancer* 13 (11), 3234–3243. doi:10.7150/jca.76618

Torgovnick, A., Schiavi, A., Shaik, A., Kassahun, H., Maglioni, S., Rea, S. L., et al. (2018). BRCA1 and BARD1 mediate apoptotic resistance but not longevity upon mitochondrial stress in *Caenorhabditis elegans*. *EMBO Rep.* 19 (12), e45856. doi:10.15252/embr.201845856

Triantafyllou, A., Liakos, P., Tsakalof, A., Georgatsou, E., Simos, G., and Bonanou, S. (2006). Cobalt induces hypoxia-inducible factor-1alpha (HIF-1alpha) in HeLa cells by an iron-independent, but ROS-PI-3K- and MAPK-dependent mechanism. *Free Radic. Res.* 40 (8), 847–856. doi:10.1080/10715760600730810

Ventura, N., Rea, S., Henderson, S. T., Condo, I., Johnson, T. E., and Testi, R. (2005). Reduced expression of frataxin extends the lifespan of *Caenorhabditis elegans*. *Aging Cell.* 4 (2), 109–112. doi:10.1111/j.1474-9726.2005.00149.x

Ventura, N., and Rea, S. L. (2007). *Caenorhabditis elegans* mitochondrial mutants as an investigative tool to study human neurodegenerative diseases associated with mitochondrial dysfunction. *Biotechnol. J.* 2 (5), 584–595. doi:10.1002/biot.200600248

Ventura, N., Rea, S. L., Schiavi, A., Torgovnick, A., Testi, R., and Johnson, T. E. (2009). p53/CEP-1 increases or decreases lifespan, depending on level of mitochondrial bioenergetic stress. *Aging Cell.* 8 (4), 380–393. doi:10.1111/j.1474-9726.2009.00482.x

Wenger, R. H. (2002). Cellular adaptation to hypoxia: O2-sensing protein hydroxylases, hypoxia-inducible transcription factors, and O2-regulated gene expression. *FASEB J.* 16 (10), 1151–1162. doi:10.1096/fj.01-0944rev

Wijesinghe, T. P., Dharmasivam, M., Dai, C. C., and Richardson, D. R. (2021). Innovative therapies for neuroblastoma: The surprisingly potent role of iron chelation in up-regulating metastasis and tumor suppressors and down-regulating the key oncogene, N-myc. *Pharmacol. Res.* 173, 105889. doi:10.1016/j.phrs.2021.105889

Xu, D., Li, X., Shao, F., Lv, G., Lv, H., Lee, J. H., et al. (2019). The protein kinase activity of fructokinase A specifies the antioxidant responses of tumor cells by phosphorylating p62. *Sci. Adv.* 5 (4), eaav4570. doi:10.1126/sciadv.aav4570

Yang, S., Zhang, M. C., Leong, R., Mbuagbaw, L., Crowther, M., and Li, A. (2021). Iron chelation therapy in patients with low- to intermediate-risk myelodysplastic syndrome: A systematic review and meta-analysis. *Br. J. Haematol.* 197, e9–e11. doi:10.1111/bjh.17998

Zhang, H., Bosch-Marce, M., Shimoda, L. A., Tan, Y. S., Baek, J. H., Wesley, J. B., et al. (2008). Mitochondrial autophagy is an HIF-1-dependent adaptive metabolic response to hypoxia. *J. Biol. Chem.* 283 (16), 10892–10903. doi:10.1074/jbc.M800102200